

Microstructure and Mechanical Properties in Hot-Rolled Extra High-Yield-Strength Steel Plates for Offshore Structure and Shipbuilding

DONGSHENG LIU, QINGLIANG LI, and TOSHIHIKO EMI

Key parameters for a thermomechanically controlled processing and accelerated cooling process (TMCP-AcC) were determined for integrated mass production to produce extra high-yield-strength microalloyed low carbon SiMnCrNiCu steel plates for offshore structure and bulk shipbuilding. Confocal scanning microscopy was used to make *in-situ* observations on the austenite grain growth during reheating. A Gleeble 3800 thermomechanical simulator was employed to investigate the flow stress behavior, static recrystallization (SRX) of austenite, and decomposition behavior of the TMCP conditioned austenite during continuous cooling. The Kocks–Mecking model was employed to describe the constitutive behavior, while the Johnson–Mehl–Avrami–Kolmogorov (JMAK) approach was used to predict the SRX kinetics. The effects of hot rolling schedule and AcC on microstructure and properties were investigated by test-scale rolling trials. The bridging between the laboratory observations and the process parameter determination to optimize the mass production was made by integrated industrial production trials on a set of a 5-m heavy plate mill equipped with an accelerated cooling system. Successful production of 60- and 50-mm-thick plates with yield strength in excess of 460 MPa and excellent toughness at low temperature (213 K (−60 °C)) in the parent metal and the simulated coarse-grained heat affected zone (CGHAZ) provides a useful integrated database for developing advanced high-strength steel plates *via* TMCP-AcC.

DOI: 10.1007/s11661-010-0458-1

© The Minerals, Metals & Materials Society and ASM International 2010

I. INTRODUCTION

FOR highly stressed steel structures such as offshore platforms and ships, dead weight has a major influence on payload and, hence, economic performance. Oil exploration is moving into deeper sea areas, and the sizes of offshore structure are increasing. Distant transportation requires building very large container ships for improving transportation efficiency, leading to the increase of hull and associated components. Although plates produced *via* thermomechanically controlled processing (TMCP) with 355 MPa minimum yield stress are well accepted, the minimum thickness of such plates must be increased for large size members for offshore and ship building. To reduce the plate thickness, more advanced high-strength plates are required.

Recently, heavy plates equivalent to the NV-E/F460 grades (minimum yield stress $R_{eH} = 460$ MPa) and NV-D/E/F500 (minimum yield stress $R_{eH} = 500$ MPa) grades (defined by Det Norske Veritas, *i.e.*, Norway

Ship Classification Society) treated by TMCP were developed for the construction of ships and drilling platforms.^[1–5] The adoption of the 60-mm-thick plates in 460 MPa yield strength class developed by JEF Steel Corporation (West Japan Steel Works, Fukuyama, Japan) has replaced conventional 80-mm-thick plates, leading to lighter weight and lower center of gravity of the superlarge container ship and with reduced construction cost and improved work efficiency.^[2] In AG der Dillinger Hüttenwerke (Dillingen, Germany),^[3] steel plates in NV-D/E/F500 grades with maximum thickness of 75 mm were used for shipbuilding such as *Mayflower Resolution*. The extra high-strength steels reduced structural thickness, reduced the vessel's deadweight, increased higher payload, and guaranteed ductility and toughness in cold waters. The production of heavy steel plates for shipbuilding requires advanced technologies covering clean steel and homogenous slab followed by TMCP and accelerated cooling process (AcC).

Although the fundamentals of metallurgical phenomena during TMCP-AcC are well understood, optimizing integrated process specifications requires accurate descriptions of the entire microstructural evolution process and resultant mechanical properties of the steel plates in industrial production. Here, more data are required to reinforce databases that enable physical metallurgy knowledge to be translated into process parameter windows for industrial production. The production of NV-F460 class TMCP-treated heavy-thickness (*e.g.*, up to 60 mm) steel plates with

DONGSHENG LIU, Senior Researcher, and TOSHIHIKO EMI, Director, are with the Institute of Research of Iron and Steel, Shasteel, Jinfeng Town, Zhangjiagang City, Jiangsu Province, 215625, People's Republic of China. Contact e-mail: dongshengliu@gmail.com
QINGLIANG LI, formerly Assistant Researcher, Institute of Research of Iron and Steel, Shasteel, is Production Engineer, Bekaert Binjiang Steel Cord Co. Ltd., Jiangyin City, Jiangsu Province 215625, People's Republic of China.

Manuscript submitted March 31, 2010.

Article published online December 3, 2010

well-balanced strength and low-temperature toughness across the entire thickness section is particularly challenging when the maximum continuously cast (CC) slab thickness and mill configuration are limited. In the present work, austenite grain growth during reheating, hot deformation, and static recrystallization (SRX) kinetics of austenite were studied in a low carbon microalloyed SiMnCrNiCu plate steel. Mathematical models for the constitutive behavior and the SRX kinetics were established. Phase transformation behavior relevant to the industrial AcC process was also studied. Integrated industrial rolling trials were conducted to produce thick plates with minimum yield strength of 460 MPa and assured minimum Charpy V-notch (CVN) toughness of 233 J, even at 213 K (−60 °C) for the 60-mm thickness.

II. EXPERIMENTAL

The chemical composition of the subject steel is characterized by low carbon content (0.07 wt pct) with balanced additions of alloy elements (chromium, nickel, and copper) and microalloying elements (niobium, vanadium, and titanium), as shown in Table I. Carbon equivalent of 0.40 and P_{cm} value of approximately 0.18 were chosen to maximize weldability. Slabs of 320-mm thickness were produced by an integrated system consisting of a basic oxygen furnace (BOF), ladle furnace (LF), Ruhrstahl–Hereus (RH), and continuous casting to secure sufficient reduction to final plate thickness of 60 to 50 mm. Measures were taken to achieve sufficient steel cleanliness to achieve the demanding toughness.^[6] Soft reduction ensured reduced center segregation in the slabs. The slabs were used for test-scale and industrial rolling trials. The plates, TMCP-AcC processed in a four-high 5-m width heavy plate mill shop, were used for austenite grain growth and thermomechanical simulations.

To obtain suitable austenite grain sizes for subsequent deformation and transformation tests, a sample was sectioned from the plate and machined into a disc (3.8-mm diameter × 3-mm height), mirror polished and set into a high-purity alumina crucible (4.5-mm inner diameter × 5-mm height). The grain growth during heating was observed *in situ* by a confocal scanning laser microscope.^[7–9] The sample and crucible were placed into the gold image furnace and heated at 5 K/s (5 °C/s) to desired temperatures in high-purity argon, preventing any oxidation. The microstructural change with temperature and time after ferrite-to-austenite transformation was observed and recorded for final analysis. Austenite grain sizes were measured as equivalent area diameter (EQAD) using the Jeffries method.^[10] Volumetric grain sizes were obtained by multiplying the measured EQAD with a factor of 1.2.^[11]

Flow stress behavior and the SRX kinetics of austenite and austenite decomposition during continuous cooling transformation (CCT) were studied with a Gleeble 3800 thermomechanical simulator (Dynamic System Inc, Poestenkill, NY),^[12] as shown in Table II.

A two-high reversing mill, 750-mm diameter × 550-mm width and rolling speed 1 m/s with AcC system, was employed for test-scale rolling. The industrial CC slabs were sectioned to 160-mm height × 150-mm width × 250-mm length. The height direction of the subslab was parallel to the through-thickness direction of the original CC slab. Each sectioned slab was soaked at 1523 K (1250 °C) for 2 hours and rolled from 160 to 18 mm in 11 passes. The average reduction ratio per pass was 0.18 to 0.2, except for the last pass, which was 0.10. The interpass time averaged 10 seconds, except for the 300-second delay time between the roughing ($T_{RR} = 1273$ to 1423 K (1000 to 1150 °C)) and finishing ($T_{FR} = 1103$ to 1153 K (830 to 880 °C)) rolling passes. Three processes were employed. Process 1: low roughing reduction ratio ($\Sigma_R = 60$ pct) coupled with

Table I. Chemical Composition of the Investigated Steel (Weight Percent)

C	Si	Mn	P	S	Al	Nb + V + Ti	Cr + Cu + Ni
0.07	0.23	1.45	0.008	0.009	0.042	0.092	0.60

Table II. Process Parameter Range Employed in the Thermomechanical Simulations

Test Series	Objective	Operating Parameter Range
Single hit tests	constitutive behavior	reheat up to 1423 K (1150 °C), hold for 5 min deformation temperature: 1023 K to 1373 K (750 °C to 1100 °C) hit strain rate: 0.1 to 10 s ^{−1}
Double hit tests	SRX	reheat up to 1423 K (1150 °C), hold for 5 min deformation temperature: 1123 K to 1373 K (850 °C to 1100 °C) first hit strain: 0.2 to 0.5 hit strain rate: 0.1 to 10 s ^{−1}
Transformation	austenite decomposition kinetics during continuous cooling	reheat up to 1423 K (1150 °C), hold for 2 min deformation temperature: 1123 K (850 °C) strain: 0 to 0.55 strain rate: 1.0 s ^{−1}

high finishing reduction ratio ($\Sigma_F = 72$ pct). Process 2: intermediate roughing reduction ratio ($\Sigma_R = 68$ pct) coupled with similar level of finishing reduction ratio ($\Sigma_F = 65$ pct). Process 3: high roughing reduction ratio ($\Sigma_R = 74$ pct) followed by low finishing reduction ratio ($\Sigma_F = 57$ pct). After finish rolling, the plates were cooled in the AcC facilities. The plate surface temperatures were monitored using an UX 70P portable radiation thermometer.

In industrial production, 60- and 50-mm-thick plates were rolled from the 320-mm CC slabs with the 5-m plate mill. After reheating the slab at 1523 K (1250 °C), the slab was subjected to descaling, rough rolling, delay, finish rolling, lamellar water flow cooling, hot leveling, and ultrasonic detection.

Tensile properties and CVN impact properties in the transverse-direction (TD) at the center thickness ($t/2$) were tested for the test plant rolled plates, while those for industrially rolled plates were tested in both the TD and longitudinal (RD) directions at $t/2$ and quarter thickness ($t/4$). Round tensile samples with 12- and 14-mm gage diameters were machined for the test plant rolled and industrially rolled plates; the tensile samples were tested at room temperature using a crosshead speed of 5 mm/min on a tensile machine (model Instron 5585, Instron Corp., Canton, MA) with 250-kN capacity. For the 60- and 50-mm-thick plates, the Z-direction properties were tested in accordance with ASTM A770 using 10-mm-diameter tensile specimens. Drop-weight testing in accordance with ASTM E208 was employed to determine the nil-ductility transition temperature (T_{NDT}) for P2-type samples. Full size CVN specimens were prepared with the notch parallel to the thickness (ND) direction and impact energy was measured from 253 K to 193 K (−20 °C to −80 °C).

The coarse-grained heat affected zone (CGHAZ) adjacent to the fusion line has the lowest toughness within the HAZ because of large prior austenite grains.^[13,14] To investigate the microstructure and properties of the CGHAZ, rectangular specimens of $10 \times 10 \times 75$ mm were made from the 50- and 60-mm-thick plates in the central 10-mm section of the plates. The CGHAZ simulations were performed using the Gleeble 3800 thermomechanical simulator employing the Rykalin-3D (thick plate) heat-transfer model. A Pt-10 pct Rh thermocouple was spot welded at the central length of the specimens for recording the temperature. The specimens were heated at 130 K/s (130 °C/s) to 1623 K (1350 °C) and held for 0.1 seconds, corresponding to the region adjacent to the fusion zone of the weldment. The specimens were subsequently cooled at approximately 50 and 15 K/s (50 and 15 °C/s) for the stipulated range of 1073 K to 573 K (800 °C to 300 °C) to be equivalent to a weld heat input of 1.5 to 5.0 kJ/mm, as shown in Figure 1. CVN specimens were made with the notch at the central length, *i.e.*, the spot-welded thermocouple position along the original ND-RD orientation of the plates, and the impact energy was measured at 213 K (−60 °C). The transformation kinetics and microstructure under the simulated CGHAZ conditions were studied using the dilatometric technique described earlier.

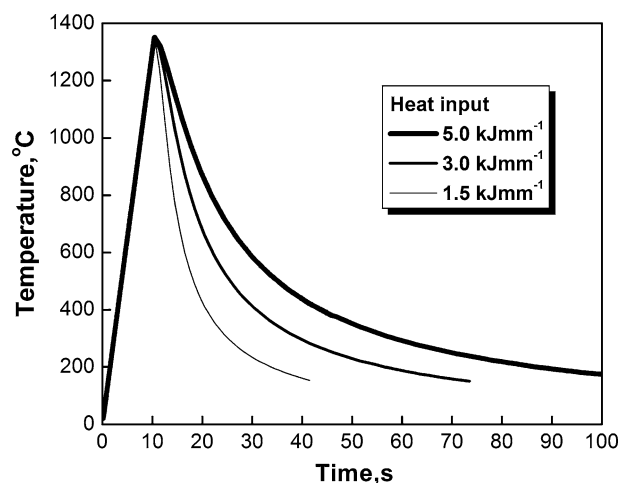


Fig. 1—Thermal profiles obtained during CGHAZ simulations in the investigated steel.

The polished specimens were etched in a 4 pct nital solution and observed with an optical microscope and a scanning electron microscope (SEM), FEI's model Quanta 3D FEG (FEI Electron Optics B. V./FEI, Czech Republic). For the CCT samples, the central plane perpendicular to the length direction was examined. For the test-scale rolled plates, the polished surface along the ND-RD orientation at $t/2$ was examined, while those along the ND-RD orientation at $t/4$ and $t/2$ were examined for the 60- and 50-mm industrial plates. These samples were also subjected to Vickers microhardness testing using a 1000 g load.

III. RESULTS AND DISCUSSION

A. Austenite Grain Growth

For 5 minutes of isothermal holding, the volumetric austenite grain size ranged from 12 μm at 1223 K (950 °C) to 60 μm at 1423 K (1150 °C). Average grain size increased to 100 μm when the holding temperature was raised to 1523 K (1250 °C). Abnormal austenite grain growth was observed above 1423 K (1150 °C). Representative austenite microstructures observed during isothermal holding are shown in Figure 2. Table III summarizes the reheating conditions and associated austenite grain sizes of specimens that were employed for subsequent deformation and transformation tests.

B. Constitutive Deformation Behavior of Austenite

The stress-strain behavior of austenite was experimentally investigated with a series of uniaxial compression tests, where the deformation temperatures (1023 K to 1373 K (750 °C to 1100 °C)) and strain rates (0.1 s^{-1} to 10 s^{-1}) were systematically varied for the initial volumetric austenite grain size of 60 μm . The flow stress increased with decreasing temperature (T_{def}) and increasing strain rate ($\dot{\epsilon}$), as shown in Figure 3. A peak in the flow stress curve at the highest deformation temperature is an indication of dynamic recrystallization, as shown in Figure 3(a).

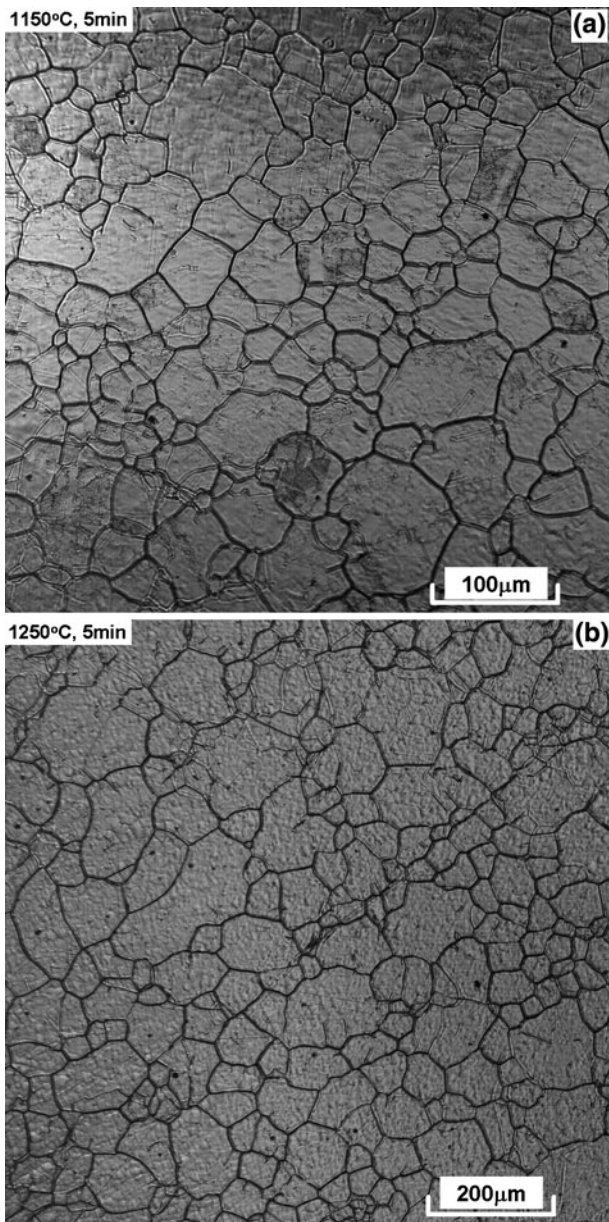


Fig. 2—Austenite microstructures formed at (a) 1423 K (1150 °C) and (b) 1523 K (1250 °C).

Table III. Reheat Conditions and Resulting Austenite Grain Sizes

Soaking Temperature, T (°C)	Austenite Grain Size (EQAD) (µm)	Volumetric Austenite Grain Size (µm)
1223 (950)	10	12
1373 (1100)	34	41
1423 (1150)	50	60
1523 (1250)	83	100

The constitutive behavior of austenite prior to the onset of dynamic recrystallization can be described.^[12,15–17] The flow stress, σ , is represented by

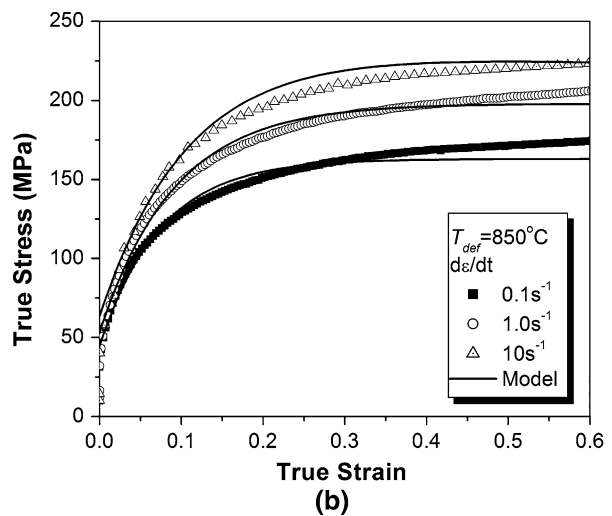
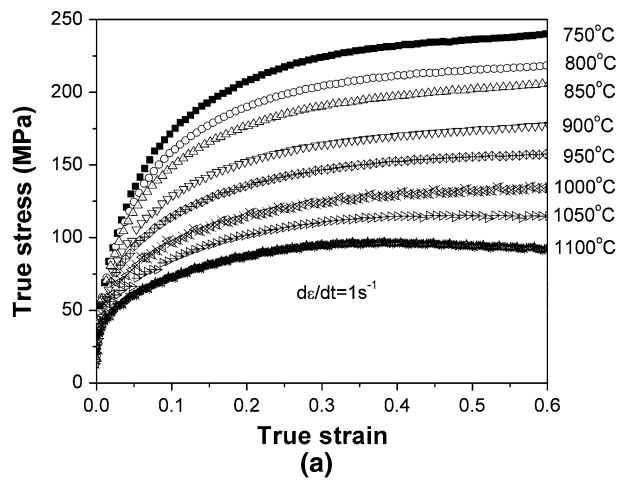


Fig. 3—(a) Effect of deformation temperature on flow stress behavior and (b) comparison between modeling and experimental results showing the effect of strain rate on the constitutive behavior.

the sum of a yield stress $\sigma_y(T, \dot{\epsilon})$ and a work hardening stress $\sigma_d(T, \dot{\epsilon}, \epsilon)$ as

$$\sigma = \sigma_y(T, \dot{\epsilon}) + \sigma_d(T, \dot{\epsilon}, \epsilon) \quad [1]$$

The temperature and strain rate dependence of the yield stress can be written as^[12]

$$\frac{\sigma_y}{\mu} = \frac{\sigma_{y0}}{\mu_0} \left\{ 1 - \left(\frac{kT}{g'_0 \mu \mathbf{b}^3} \ln \frac{\dot{\epsilon}_0}{\dot{\epsilon}} \right)^{1/2} \right\}^2 \quad [2]$$

where μ is the temperature-dependent shear modulus,^[18] μ_0 is the shear modulus at 0 K (−273 °C), kT has its normal meaning, and \mathbf{b} is the magnitude of the Burgers vector. The normalizing strain rate can be postulated at $\dot{\epsilon}'_0 = 10^7 \text{ s}^{-1}$, and g'_0 , and σ_{y0} (the extrapolation of the yield stress to 0 K (−273 °C)) are taken as adjustable parameters.

The work hardening stress is given by

$$\sigma_d = \sigma_v \left(1 - \exp\left(-\frac{\theta_0}{\sigma_v} \epsilon\right) \right) \quad [3]$$

Table IV. Parameters Describing Constitutive Behavior and SRX

g_0	g'_0	σ_{y0} (MPa)	σ_{v0} (MPa)	A ($\mu\text{m}^{-c_1} \text{s}^{c_3+1}$)	c_1	c_2	c_3	Q_{SRX} (kJ/mol)	n_{SRX}
1.0	1.0	456	1221	6.44×10^{-18}	1.0	-2.54	-0.3	364.8	1.0

where ε is the true strain, θ_0 the initial work hardening rate that can be approximated by $\mu/30$, and σ_v the scaling stress corresponding to the stress level at zero work-hardening rate minus the yield stress, as described by^[19]

$$\frac{\sigma_v}{\mu} = \frac{\sigma_{v0}}{\mu_0} \left\{ 1 - \left(\frac{kT}{g_0 \mu b^3} \ln \frac{\dot{\varepsilon}_0}{\dot{\varepsilon}} \right)^{1/2} \right\}^2 \quad [4]$$

where σ_{v0} is the scaling stress extrapolated to 0 K (-273 °C) that, together with g_0 , is used as an adjustable parameter. The parameters are summarized in Table IV. Here, $g'_0 = g_0 = 1$ may be introduced as the universal relationship independent of steel composition. Thus, only the extrapolations of yield stress and scaling stress at 0 K (-273 °C) remain as composition-dependent parameters, as observed previously for DP,^[15] TRIP,^[12] and CP^[16] steels. Fit quality is illustrated in Figure 3(b), showing the effect of strain rate on the flow stress behavior.

C. SRX Kinetics and Grain Size

Both the austenite microstructure at the start of finish rolling and the level of pancaking attained after finish rolling have great influence on the austenite decomposition kinetics and, therefore, the resultant microstructure and mechanical properties of the plate. For rough rolling of a typical shipbuilding plate in the 5-m plate mill, the strain rate ranged from 1 to 2 s⁻¹ and the maximum effective pass strain was 0.2, which is less than the observed peak strain, as shown in Figure 3. Under the rough rolling conditions for the investigated steel, therefore, SRX should be the dominant softening mechanism for which the solute drag mechanism of microalloying elements is taken into account at temperatures higher than 1123 K (950 °C). The fraction of recrystallized austenite was quantified by established procedures,^[12] and the SRX kinetics can be described using the Johnson–Mehl–Avrami–Kolmogorov (JMAK) approach:^[20]

$$F_{\text{SRX}} = 1 - \exp\left(-0.693 \left(\frac{t}{t_{50}}\right)^{n_{\text{SRX}}}\right) \quad [5]$$

where F_{SRX} is the recrystallized fraction, n_{SRX} is the Avrami exponent, and t_{50} is the time for 50 pct recrystallization. The parameter, t_{50} , is the time for 50 pct recrystallization and can be represented as a function of temperature (T), initial austenite grain size (d_γ), applied strain (ε), and strain rate ($\dot{\varepsilon}$) as^[21]

$$t_{50} = A d_\gamma^{c_1} \varepsilon^{c_2} \dot{\varepsilon}^{c_3} \exp\left(\frac{Q_{\text{SRX}}}{RT}\right) \quad [6]$$

where Q_{SRX} is an effective activation energy for recrystallization; R is the ideal gas constant; and A , c_1 , c_2 , and

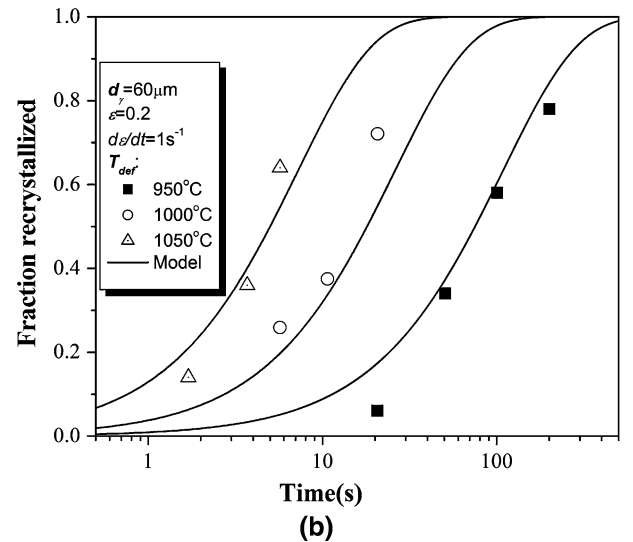
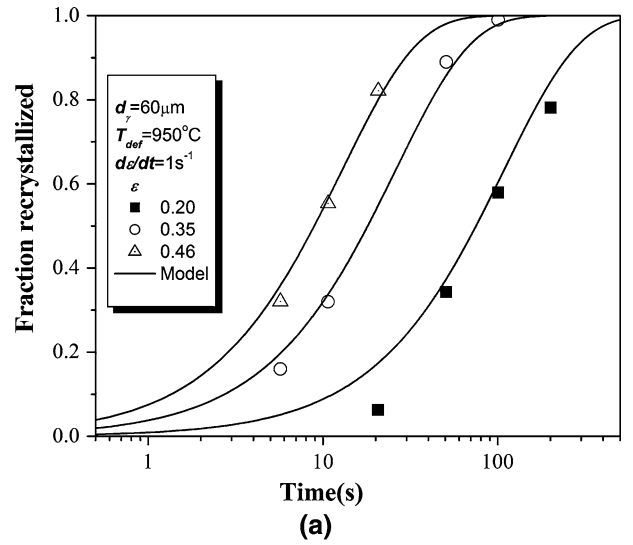


Fig. 4—Comparison of SRX kinetics measured and modeled showing (a) the effect of strain and (b) the effect of deformation temperature.

c_3 are constants. The parameters for t_{50} and the Avrami exponent n_{SRX} were determined, as summarized in Table IV. The effect of temperature and strain on the SRX kinetics are presented in Figure 4. Furthermore, for the start of finish rolling at 1223 K (950 °C) or below, austenite recrystallization cannot complete during the pass interval, which is normally 10 seconds according to the present results. Strain accumulation (pancaking) can be achieved in this region.

This is further confirmed by the interrupted compression experiments conducted at 1173 K and 1123 K (900 °C and 850 °C), as shown in Figure 5, indicating the measured fractions of softened (f_s) materials and

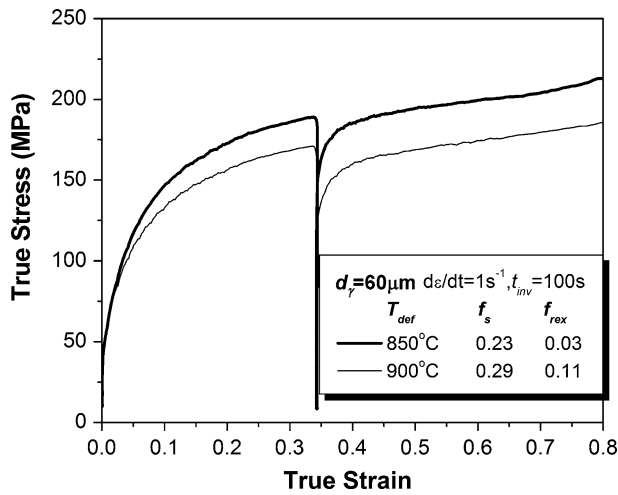


Fig. 5—Stress-strain curves measured by double hit compression tests.

recrystallized (f_{rex}) austenite grains even 100 seconds after the first hit deformation. The achievement of deformed nonrecrystallized austenite by finish rolling is critically important for enhancing the transformation of acicular ferrite (AF)^[22] during AcC, which offers the best combination of strength and toughness.^[23,24]

An important characteristic of recrystallization is the resulting grain size; grain refinement from pass to pass occurs as long as complete recrystallization is possible. Revealing the recrystallized grain size for the present low carbon steels proved to be a challenging task; estimates of the grain sizes indicated that they are similar to those observed in steels with higher carbon and alloy levels. The model of recrystallized grain size (d_{SRX} in μm) for Nb microalloyed steels is recommended,^[25] for the present steel, to be

$$d_{SRX} = K \cdot d_0^m \cdot \varepsilon^{-\nu} \quad [7]$$

where K is at 0.9 to 1.9 (here, $K = 1.0$ was selected), $m = 0.65$, and $\nu = 0.67$. The grain size after growth (d_g) becomes

$$d_g = \left[d_{SRX} + k \cdot t_g \cdot \exp\left(-\frac{Q_g}{RT}\right) \right]^{\frac{1}{u}} \quad [8]$$

where t_g is the time after the recrystallization is complete, $k = 4.1$, $u = 4.5$, and $Q_g = 435$ kJ/mol.

However, further studies are required to more accurately quantify recrystallized grain sizes for lower carbon steels. Such investigations may include novel characterization techniques such as laser ultrasonics.^[16,26,27] The present study, however, offers predictive tools to describe austenite evolution during hot rolling for the investigated steel.

D. CCT Behavior and Microstructure

CCT tests were conducted for initial austenite microstructures with volumetric grain sizes of 12, 41, and 60 μm . The strains (ε) applied at 1123 K (850 °C) under nonrecrystallization conditions are 0, 0.3, and 0.55; the

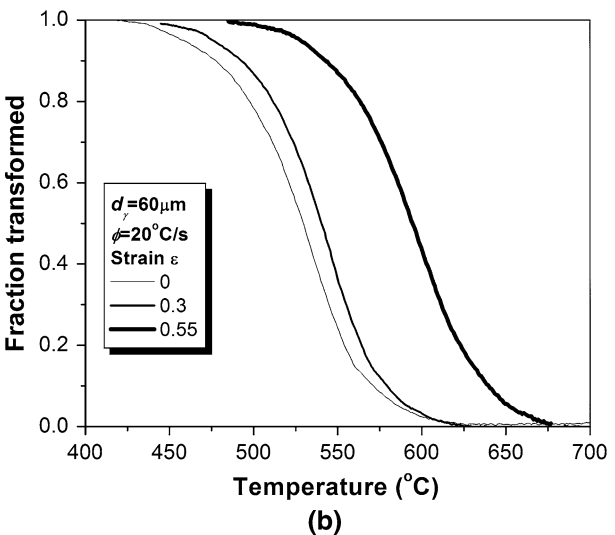
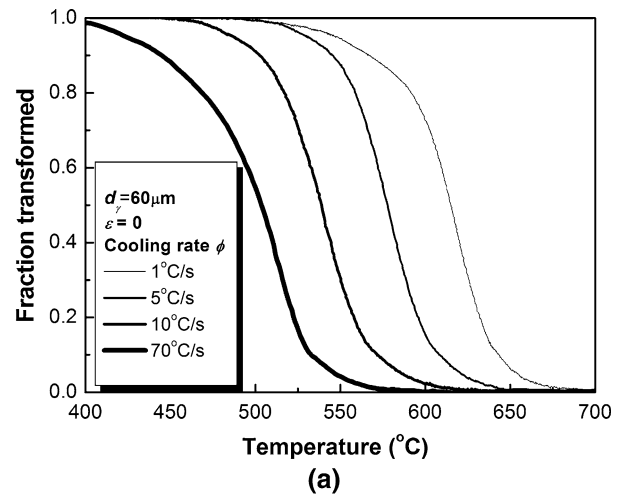


Fig. 6—Experimental results showing the effects of (a) cooling rate (ϕ) and (b) pancaking (ε) on CCT behavior.

cooling rates (ϕ) employed ranged from 1 to 70 K/s (1 to 70 °C/s). The cooling rates cover the industrially applicable parameters in heavy plate production in Shasteel, 30 K/s (30 °C/s), 20 K/s (20 °C/s), and 10 K/s (10 °C/s), for 20-, 30-, and 50-mm-thick plates, respectively. Figure 6 gives the typical experimental results showing the effect of cooling rate (Figure 6(a)) and austenite pancaking (Figure 6(b)) on CCT curves. The transformation shifted to lower temperatures with increasing cooling rate and shifted to a higher temperature range with the increasing austenite pancaking. The transformation products are shown in Figure 7. The entire bainite microstructure formed during continuous cooling at 5 to 70 K/s (5 to 70 °C/s) in the nondeformed austenite. When the cooling rate slowed to 5 K/s (5 °C/s), coarse martensite/austenite (M/A) constituents associated with the ferrite matrix, *i.e.*, granular bainite (GB) and upper bainite (UB), are dominant, as shown in Figure 7(a). When the cooling rate is high at 20 K/s (20 °C/s), refined lathlike bainite (LB) microstructures, and reduced fraction of UB + GB are the majority phases, resulting in higher hardness, as shown

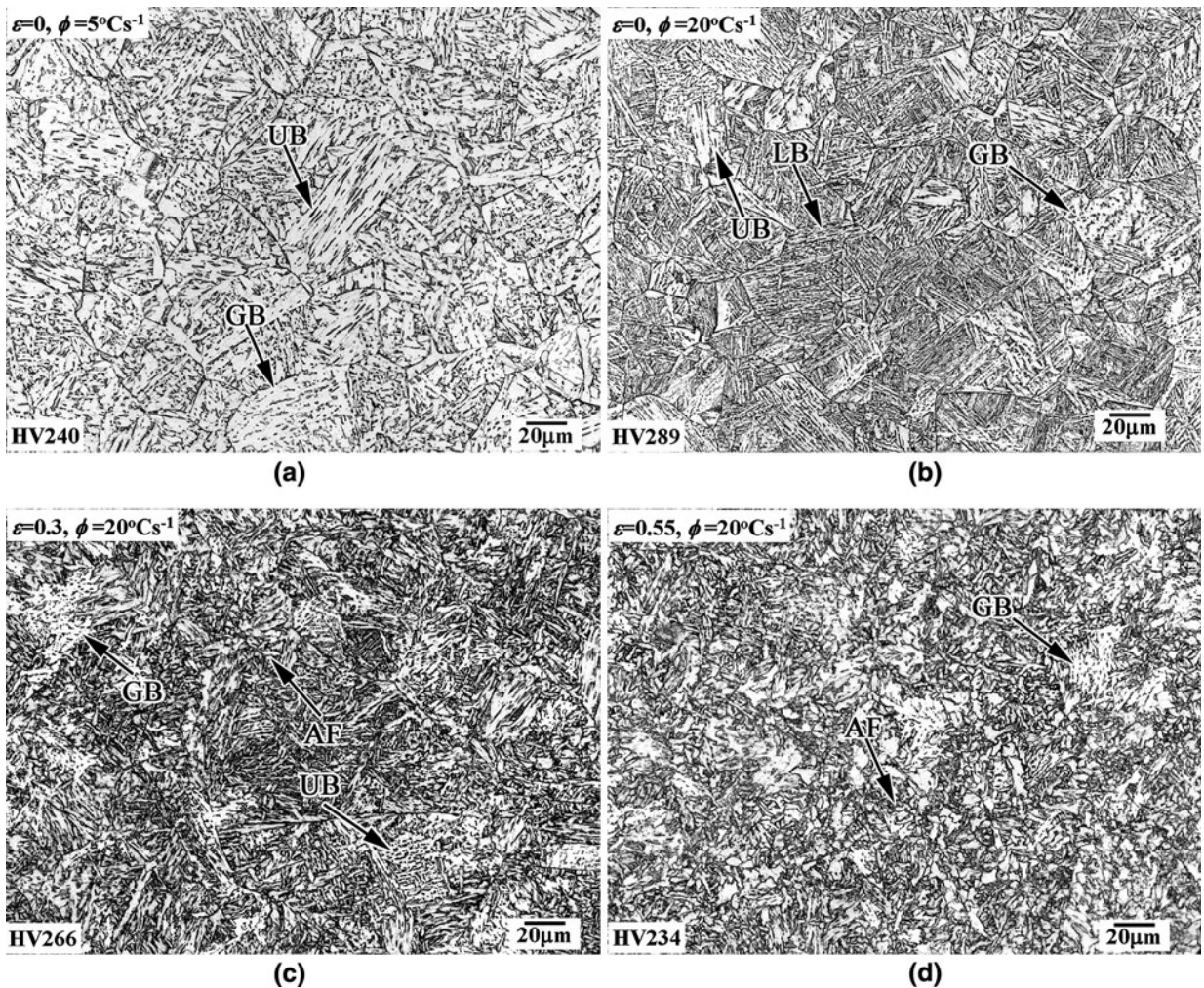


Fig. 7—Microstructures produced during CCT with different cooling rates (ϕ) and austenite pancaking (ϵ).

in Figure 7(b). The role of austenite pancaking on the transformed microstructure is illustrated in Figures 7(b) through (d) at 20 K/s (20 °C/s). About 20 pct of AF and 80 pct of UB were observed when true strain of 0.3 was applied in the austenite nonrecrystallization region, prior to phase transformation. The increased strain of 0.55 in the austenite resulted in predominantly an AF microstructure with the presence of a minor amount fine-grained polygonal ferrite (PF) and GB. A similar microstructure was observed at the same austenite condition as in Figure 7(d), but at a continuous cooling rate of 10 K/s (10 °C/s). This fact indicates that the resultant microstructure is insensitive to the fluctuation of cooling rate within 10 to 20 K/s (10 to 20 °C/s), and hence, a robust AcC process can be applied to the thermomechanically conditioned austenite to achieve the desired microstructure.

E. Microstructures and Mechanical Properties Achieved in the Test-Scale Rolling Trials

Two-stage rolling, *i.e.*, hot deformation in the austenite recrystallization region and the nonrecrystallization region, followed by AcC conditions, was selected

for simulations conducted with a test rolling mill equipped with a runout table AcC system. Table V summarizes the processing parameters employed in the trials. After simulated rough rolling, the austenite microstructure is recrystallized according to the developed SRX kinetics model and the rolling schedules.

The level of pancaking during finish rolling and the cooling processes are the dominant factors for the resultant microstructures. Figure 8 shows the microstructures produced in the test rolled steel plates. For process 1, with the most aggressive finish rolling of 72 pct reduction, a mixture of PF grains with grain size of 2 to 6 μm and AF and M/A islands were produced, as shown in Figure 8(a). Dominant AF grains including 7.7 pct UB associated with M/A and fine-grained equiaxed ferrite were produced for process 2 (Figures 8(b) and (c)). The volume fraction of PF decreased with increasing cooling rate (ϕ), decreasing finish cooling temperature (T_{FC}), and decreasing total finishing reduction (Σ_F) in austenite, which in turn decreases the driving pressure for the ferrite transformation. A significant amount of UB (17.4 pct), which is detrimental to toughness, is presented (Figure 8(d)) in the sample by process 3. The microstructure variation

Table V. Processing Parameters Employed in the Test-Scale Rolling Trials

Proc.	Thickness <i>t</i> (mm)	Rough Rolling		Finish Rolling		Accelerated Cooling		
		T_{RR} , K (°C)	Σ_R (Pct)	T_{FR} , K (°C)	Σ_F (Pct)	ϕ , K/s (°C/s)	T_{SC} , K (°C)	T_{FC} , K (°C)
1	18.0	1323 to 1263 (1050 to 990)	56.0	1143 to 1133 (870 to 860)	72.0	10.0 (10.0)	1123 (850)	823 (550)
2	18.0	1323 to 1273 (1050 to 1000)	64.0	1153 to 1133 (880 to 860)	65.0	15.0 (15.0)	1123 (850)	673 (400)
3	18.0	1423 to 1363 (1150 to 1090)	71.0	1143 to 1103 (870 to 830)	57.0	7.0 (7.0)	1123 (850)	823 (550)

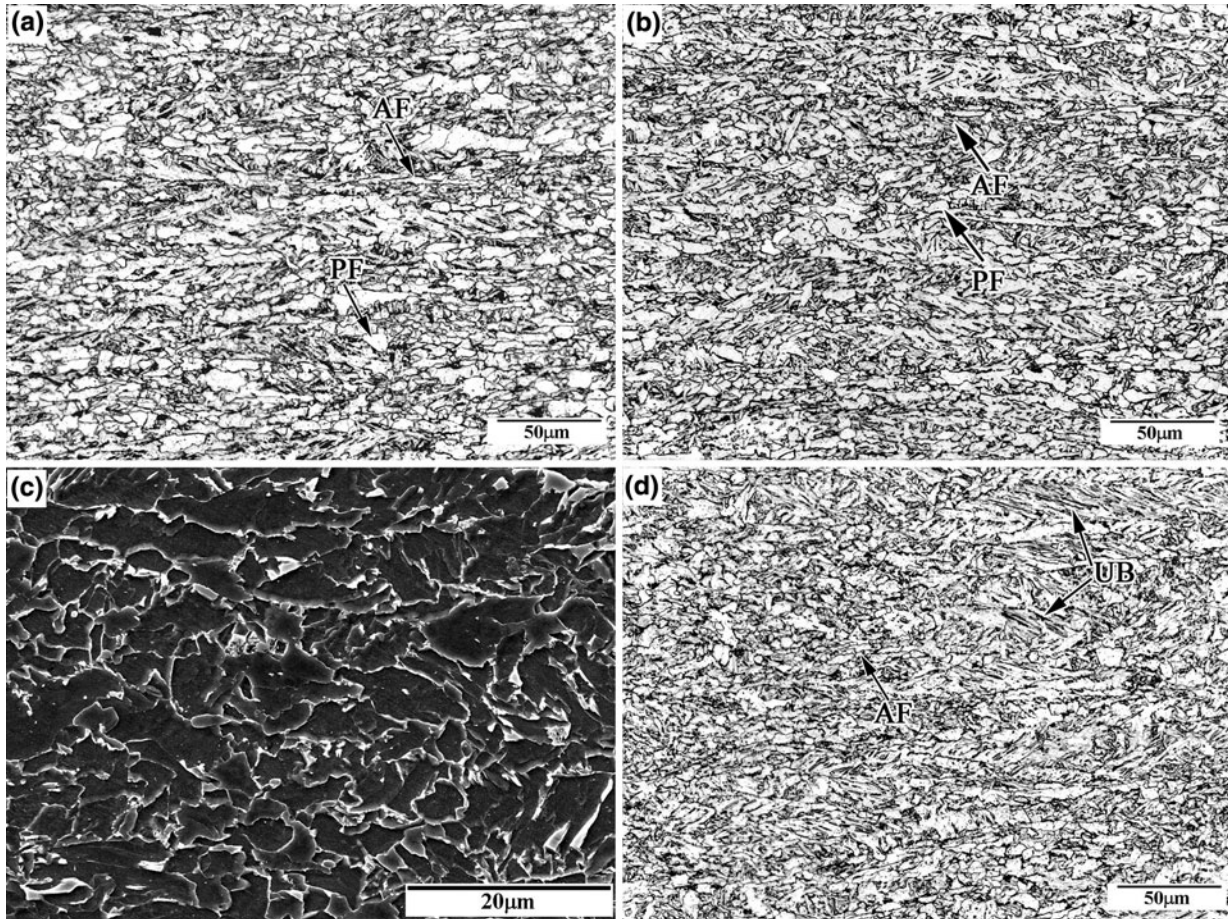


Fig. 8—Microstructures produced during the test-scale rolling trials in the samples treated by (a) process 1, (b) and (c) process 2, and (d) process 3.

Table VI. Mechanical Properties of the Plates Produced by the Pilot Scale Rolling Trials

Proc.	Tensile Properties			CVN Impact Energy (J)		
	$R_{p0.2}$ (MPa)	R_m (MPa)	A_5 (Pct)	233 K (−40 °C)	213 K (−60 °C)	193 K (−80 °C)
1	541	649	24	321, 359, 321, ave. 334	345, 358, 355, ave. 353	299, 269, 355, ave. 306
2	538	666	24	344, 286, 272, ave. 301	340, 361, 269, ave. 323	209, 292, 315, ave. 272
3	477	638	28	259, 292, 307, ave. 285	212, 173, 139, ave. 208	86, 35, 37, ave. 53

observed in the test-rolled materials is consistent with those observed in the CCT studies, as shown in Figure 7. The increase of pancaking promotes the formation of PF and AF and decreases the fraction of UB. Table VI summarizes the mechanical properties of

the as-rolled plates. The yield/tensile strength and the ductility of the experimental steel plates by processes 1 and 2 exceed the minimum requirement for the F460 grade and meet the requirement for F500 grade. The CVN toughness is excellent even at 193 K (−80 °C).

The formation of UB by process 3 deteriorates the room-temperature strength and low-temperature (193 K (−80 °C)) toughness.

Han *et al.*^[23,24] found that the grain-boundary misorientation in coarse high-temperature transformed bainite is low, and hence, the effective grain size is large; this condition decreases the low-temperature toughness in the thermomechanically processed high-strength steels. The fraction of fine-grained AF microstructure is high in the present study, leading to decreased effective grain size and improved low-temperature toughness. The present study emphasizes an integrated thermomechanical rolling scheme consisting of applying substantial reduction ratio (in excess of 65 pct) in the austenite nonrecrystallization region and accelerated cooling at 10 to 20 K/s (10 to 20 °C/s) with an interrupted cooling temperature no higher than 823 K (550 °C), to achieve fine-grained ferrite and AF in the shipbuilding steel.

F. Microstructures and Mechanical Properties Achieved in Industrial Production

After the laboratory trials, the optimum TMCP parameters were established for industrial production of the 60- and 50-mm-thick plates. The temperatures and total accumulated reduction ratios during finishing rolling, starting, and ending temperatures of accelerated cooling and cooling rate are critical steps in the industrial processing. The 320-mm-thick industrial slabs with the composition shown in Table I were used for these trials. To produce the 60-mm plate, the slab with the 100- μm austenite grain size was refined by five-pass rough rolling starting at 1298 K (1025 °C) and ending at 1256 K (983 °C), as measured on the plate surface. The central temperatures, however, were estimated starting at 1422 K (1149 °C) and ending at 1405 K (1132 °C). The effective pass strains during roughing rolling were 0.13, 0.14, 0.19, 0.19, and 0.16. Equations [5] through [8] were integrated and the fraction and grain size of recrystallized austenite were calculated. A recrystallized austenite grain size of 36.5 μm at the exit of pass 5 was calculated. The austenite microstructure was then coarsened during delay, resulting in approximately 60.0- μm grains at the entry of finishing rolling. A similar austenite microstructure was estimated for the 50-mm plate at the entry of finishing rolling. The finishing rolling reduction ratio in the austenite nonrecrystallization region was greater than 63 pct for both 60- and 50-mm-thick plates. The thermomechanically rolled plates underwent accelerated cooling at about 10 K/s (10 °C/s), starting from 1073 K (800 °C), interrupted at 753 K (480 °C), followed by hot leveling and air cooling.

Figure 9 shows the optical microscope and SEM images of the microstructures at $1/4t$ and $1/2t$ on the ND \times RD sections in the as-rolled 60- and 50-mm plates. The microstructures consisted of fine-grained PF and AF and second phase, which is identified by SEM as M/A phase. Some UB grains were also observed in the 50-mm plate. Table VII summarizes the mechanical properties of the plates in the as-hot-rolled condition and the strain aging condition. Excellent strength, ductility, and

low-temperature toughness were achieved for the industrially as-rolled plates. These results confirm the validity of the key processing parameters determined in the laboratory studies. However, the strength and toughness near the plate surface are generally higher than those in the central area. The minimum yield strength and tensile strength attain 463 and 588 MPa in the central section of the 60-mm plate, satisfying the specification for F460 grade (minimum $R_{cH} = 460$ MPa, $R_m = 570$ MPa, and $A_5 = 17$ pct). The tensile properties in the 50-mm plate are well above the F460 specification and nearly reach the specification for F500. Excellent properties in the Z direction (ψ_Z) were also observed in both cases during tensile tests. The T_{NDT} values measured for the 60- and 50-mm plates are 183 K and 188 K (−90 °C and −85 °C), indicating the ductile nature of the plates at 213 K (−60 °C). In fact, CVN tests at 213 K (−60 °C) exhibited a minimum 233 J for the 60-mm plate and 121 J for the 50-mm plate, which are well above the minimum requirement of 31 J. The CVN impact toughness at $t/2$ of the 50-mm plate is inferior to that of the 60-mm plate, which may be explained by the presence of UB.

During the construction of ship hull structures, the plates are subjected to cold leveling, roll bending, press forming, *etc.* Strain aging will take place, which will result in increased strength and decreased ductility and toughness. The CVN testing, therefore, was conducted according to the procedures defined in the approval of manufacturer, and the results at 213 K (−60 °C) are also given in Table VII. The samples were taken at $t/2$ and $t/4$ of the plates and subjected to 5 pct elongation ($\epsilon_{0.05}$) parallel to the rolling direction and, subsequently, aged at 523 K (250 °C) for 1 hour. The steel plates showed excellent toughness even after strain aging.

G. Microstructure and Properties in the Simulated CGHAZ

Table VIII shows the CVN impact toughness measured under various heat input conditions. When the heat input was 1.5 to 3.0 kJ/mm, excellent toughness values were observed even at 213 K (−60 °C). At 5.0 kJ/mm, however, the impact toughness decreased substantially, not achieving the targets as defined for the parent F460-steel plates.

The effect of heat input on continuous transformation kinetics in the simulated CGHAZ is given in Figure 10. As the heat input increases, the cooling rate decreases, as shown in Figure 2, making the transformation shift to higher temperatures. Here, the martensite-start temperature (M_s) and bainite-start temperature (B_s) are estimated after Capdevila *et al.*^[28] and Lee,^[29] respectively, by

$$M_s(\text{K}) = 764.2 - 302.6C - 30.6Mn - 16.6Ni - 8.9Cr + 2.4Mo - 11.3Cu + 8.8Co + 7.4W - 14.5Si,$$

and

$$B_s(^\circ\text{C}) = 745 - 110C - 59Mn - 39Ni - 68Cr - 106Mo - 17MnNi + 6Cr^2 + 29Mo^2$$

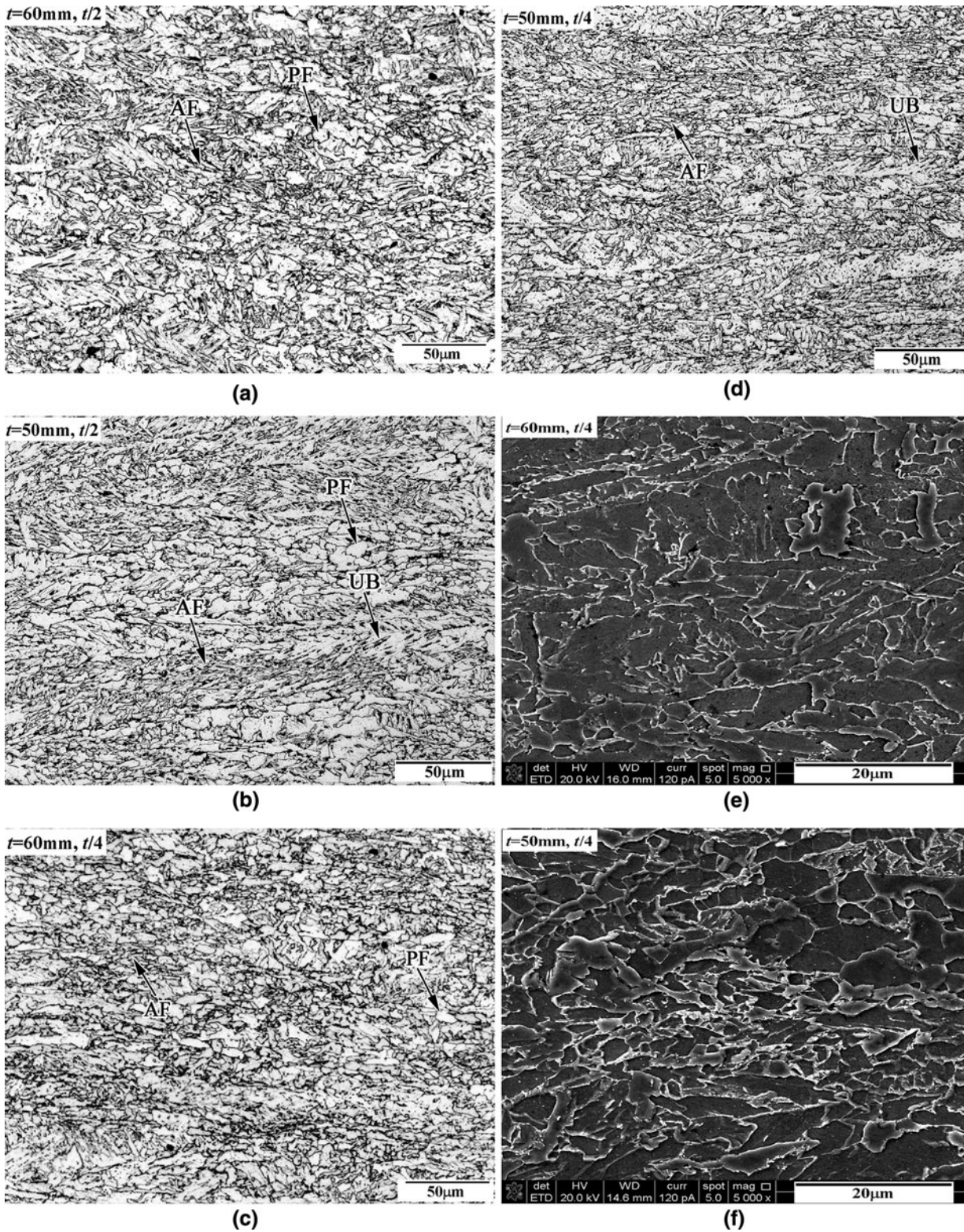


Fig. 9—Microstructures observed in the industrially produced 60- and 50-mm-thick plates at $t/4$ and $t/2$.

resulting in $M_s = 687$ K (414 °C) and $B_s = 900$ K (627 °C) for the present plates. According to Figure 10, one can estimate about 95 pct bainite and 5 pct martensite while the heat input is 1.5 kJ/mm and about

100 pct bainite at 3.0 and 5.0 kJ/mm. The microstructure and hardness at the corresponding CGHAZ are shown in Figure 11. At 1.5 kJ/mm, the microstructure is mainly LB, which corresponds to the highest hardness

Table VII. Mechanical Properties of the Industrially Produced Hot-Rolled Steel Plates

t (mm)	Location	$R_{p0.2}$ (MPa)	R_m (MPa)	A_5 (Pct)	ψ_Z (Pct)	T_{NDT} , K (°C)	CVN Impact Energy at 213 K (–60 °C) (J)		
							As Hot Rolled	$\epsilon_{0.05}$ + Aging at 523 K (250 °C) for 1 h	
60	TD-1/2 t	463	588	25	74.0	183 (–90)	310, 314, 233, ave. 285	291, 289, 266, ave. 282	
	RD-1/2 t	491	621	23			309, 233, 289, ave. 277		
	TD-1/4 t	524	639	23			276, 330, 299, ave. 302		286, 302, 296, ave. 295
	RD-1/4 t	510	620	26			310, 269, 312, ave. 300		
50	TD-1/2 t	500	632	26	77.0	188 (–85)	249, 231, 261, ave. 247	232, 197, 137, ave. 189	
	RD-1/2 t	493	622	24			187, 226, 121, ave. 178		
	TD-1/4 t	565	677	26			309, 299, 301, ave. 303		296, 307, 264, ave. 289
	RD-1/4 t	518	635	24			296, 285, 306, ave. 296		

Table VIII. Impact Toughness at 213 K (–60 °C) in the Simulated CGHAZ Conditions

Thickness t (mm)	Heat input (kJ/mm)	Peak Temperature, K (°C)	CVN Impact Energy at 213 K (–60 °C)(J)
60	1.5	1623 (1350)	239, 226, 91.0, ave. 185
60	3.0	1623 (1350)	146, 265, 93.0, ave. 168
50	1.5	1623 (1350)	238, 227, 257, ave. 240
50	3.0	1623 (1350)	295, 272, 289, ave. 285
50	5.0	1623 (1350)	30, 36, 13, ave. 26

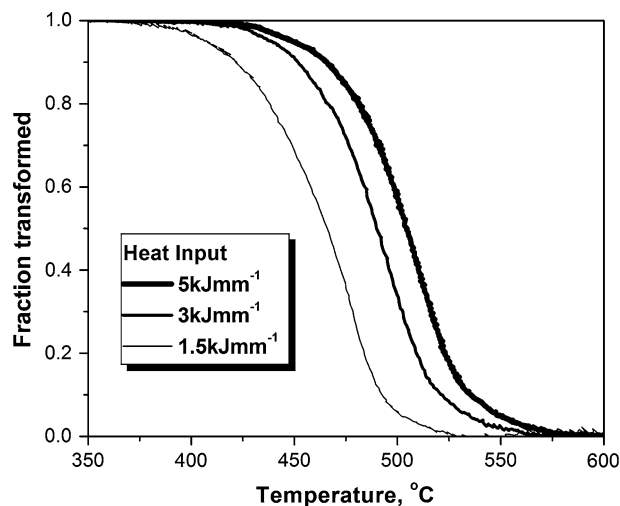


Fig. 10—Effect of heat input on CCT kinetics in the simulated CGHAZ conditions.

of 311 HV and best HAZ toughness at 213 K (–60 °C). The hardness is within the limit for the fabrication of offshore structures and icebreaker ships. At 3.0 kJ/mm, similar microstructure and hardness are observed, which lead again to excellent toughness even at 213 K (–60 °C). At 5.0 kJ/mm, however, microstructure is featured by UB and coarse M/A constituents associated with the GB matrix, leading to the lowest hardness and worst toughness.

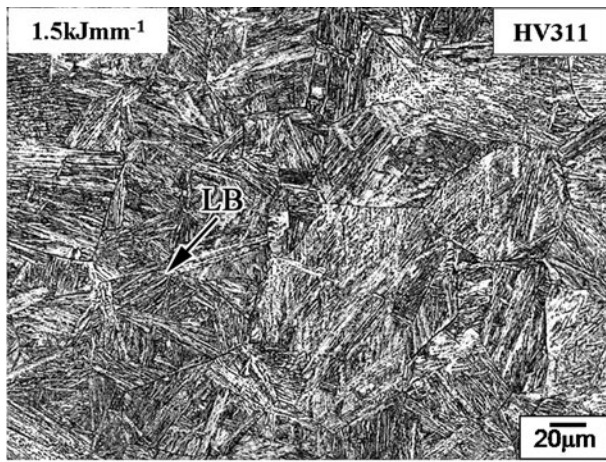
The mixture of low-temperature transformed bainite and small amount of martensite was thought to give the best toughness in the HAZ, while UB associated with M/A constituents deteriorates HAZ toughness.^[30] Miao *et al.*^[31] found that the LB microstructure has a high density of high-angle grain boundaries (≥ 15 deg

between the bainite plates formed in identical prior austenite grain and hence reduced effective grain size, which in turn enhance the ductile fracture resistance. High heat input during welding results in the formation of coarse M/A constituents associated with GB and low misorientation grain boundaries leading to large effective grain size, deteriorating the toughness in the HAZ. Miao *et al.*'s finding is consistent in nature with Han *et al.*'s observations.^[23,24] The observed effects of heat input on the properties, transformation kinetics, and microstructure in the present work indicate that the limit of heat input during welding practice for the investigated plate is 3.0 kJ/mm, which is in general agreement with the studies of welded high-strength steels.^[32]

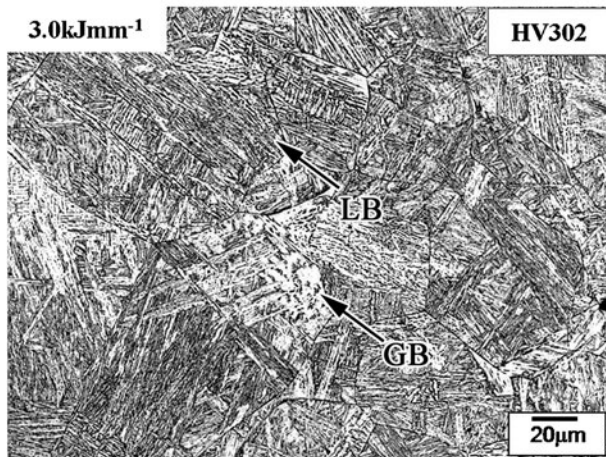
IV. CONCLUSIONS

An integrated investigation on processing, microstructure, and mechanical properties was conducted for making a 460 MPa ultra high-yield-strength class of shipbuilding steel on the basis of laboratory simulation and industrial production of low carbon SiMnCrNiCu steel. The investigation is intended to bridge laboratory scale physical metallurgy and integrated industrial TMCP-AcC, providing a database for chemical composition and process parameters for the advanced high-strength steel production.

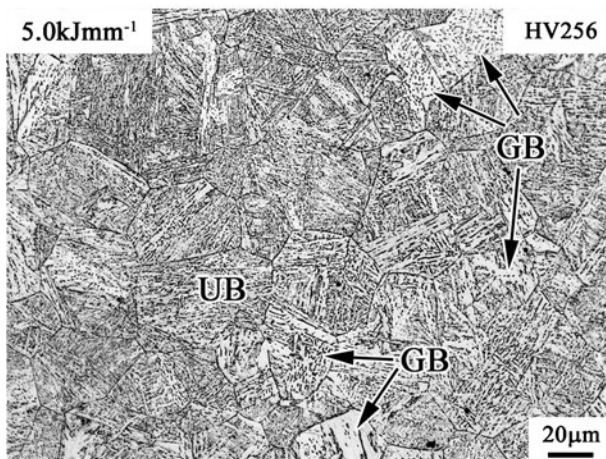
1. The stress-strain behavior of austenite during hot rolling is described by the Kocks–Mecking model for the conditions where dynamic recrystallization does not occur, while the SRX kinetics is satisfactorily described by the conventional Avrami approach. Accordingly, the austenite microstructure evolution model for the 460 MPa yield stress class thick plate steel is established.



(a)



(b)



(c)

Fig. 11—Effect of heat input on microstructures in the CGHAZ conditions.

2. CCT behavior of the thermomechanically processed austenite has revealed the AcC window; *i.e.*, the cooling rate ranged from 10 to 20 K/s (10 to 20 °C/s) and the interrupted accelerated cooling temperature was lower than 823 K (550 °C) for the formation of an

acicular microstructure after deformation in the non-recrystallization region of austenite.

3. The resultant microstructure and mechanical properties have confirmed that refined acicular ferrite microstructure must be produced to meet the minimum requirement of the strength and low-temperature toughness for the F460 plate steel. The key TMCP-AcC parameters consist of applying about 65 pct reduction ratio in the austenite nonrecrystallization region followed by the aforementioned accelerated cooling.
4. The laboratory-defined TMCP-AcC scheme has been validated by industrial trials. The industrially produced 60- and 50-mm-thick plates meet the specification for F460 grade not only in the as-rolled state, but also under more severe strain-aged condition.
5. The effect of heat input on phase transformation, microstructure, and properties of the simulated CGHAZ has been investigated. The heat input should be lower than 3.0 kJ/mm for the investigated steel to guarantee sufficient toughness at 213 K (−60 °C) at the HAZ.

ACKNOWLEDGMENTS

The authors acknowledge the financial support received from Shasteel. The authors are indebted to Ms. S. Chen and Dr. X. Zhang for arranging the hot plate rolling trials. The able assistance received from Dr. H. Zhang, Mr. B. Cheng, and Mr. H. Zhu is warmly appreciated.

REFERENCES

1. I.V. Gorynin, V.V. Rybin, V.A. Malyshevskii, and E.I. Khlusova: *Met. Sci. Heat Treatment*, 2007, vol. 49, pp. 3–9.
2. K. Ichimiya, H. Sumi, and T. Hirai: *JFE Techn. Rep.*, 2008, June 11, pp. 7–12.
3. W. Schütz and F. Schröter: *Mater. Sci. Technol.*, 2005, vol. 21, pp. 590–96.
4. N.A. McPherson: *Ironmaking and Steelmaking*, 2009, vol. 36, pp. 193–200.
5. Y. Nagai, H. Inoue, T. Nakashima, T. Adachi, H. Fukami, A. Date, and A. Kojima: *Nippon Steel Techn. Rep.*, 2004, July, No. 90, pp. 14–19.
6. Det Norske Veritas Standard: Rules for Classification of Ships/High Speed, Light Craft and Naval Surface Craft on Metallic Materials, Hovik, Norway, 2007, pp.17–26.
7. H. Yin, K. Blazek, and O. Lanzi: *ISIJ Int.*, 2009, vol. 49, pp. 1561–67.
8. N. Kikuchi, S. Nabeshima, Y. Kishimoto, T. Matsushita, and S. Sridhar: *ISIJ Int.*, 2007, vol. 47, pp. 1255–64.
9. H. Chikama, H. Shibata, T. Emi, and M. Suzuki: *Mater. Trans. JIM*, 1996, vol. 37, pp. 620–26.
10. ASTM Standard Designation E112-88, *1994 Annual Book of ASTM Standards*, ASTM, Philadelphia, PA, 1994, vol. 3.01, p. 227.
11. A. Giumelli, M. Militzer, and E.B. Hawbolt: *ISIJ Int.*, 1999, vol. 39, pp. 271–80.
12. D. Liu, F. Fazeli, M. Militzer, and W.J. Poole: *Metall. Mater. Trans. A*, 2007, vol. 38A, pp. 894–909.
13. M. Shome and O.N. Mohanty: *Metall. Mater. Trans. A*, 2006, vol. 37A, pp. 2159–69.
14. K. Banerjee and U.K. Chatterjee: *Metall. Mater. Trans. A*, 2003, vol. 34A, pp. 1297–309.
15. D. Liu, F. Fazeli, and M. Militzer: *ISIJ Int.*, 2007, vol. 47, pp. 1789–98.

16. S. Sarkar and M. Militzer: *Mater. Sci. Technol.*, 2009, vol. 25, pp. 1134–46.
17. M. Militzer and Y. Brechet: *Metall. Mater. Trans. A*, 2009, vol. 40A, pp. 2273–82.
18. H.J. Frost and M.F. Ashby: *Deformation Mechanism Maps*, Pergamon Press, Oxford, United Kingdom, 1982.
19. U.F. Kocks and H. Mecking: *Prog. Mater. Sci.*, 2003, vol. 48, pp. 171–273.
20. M. Avrami: *J. Chem. Phys.*, 1940, vol. 8, pp. 212–24.
21. M. Militzer, E.B. Hawbolt, and T.R. Meadowcroft: *Metall. Mater. Trans. A*, 2000, vol. 31A, pp. 1247–59.
22. R.Y. Zhang and J.D. Boyd: *Metall. Mater. Trans. A*, 2010, vol. 41A, pp. 1448–59.
23. S.Y. Han, S.Y. Shin, S. Lee, N.J. Kim, J.H. Bae, and K. Kim: *Metall. Mater. Trans. A*, 2010, vol. 41A, pp. 329–40.
24. S.Y. Han, S.Y. Shin, C.H. Seo, H. Lee, J.H. Bae, and K. Kim: *Metall. Mater. Trans. A*, 2010, vol. 41A, pp. 1851–62.
25. M. Jonsson: *ISIJ Int.*, 2006, vol. 46, pp. 1192–99.
26. M. Dubois, A. Moreau, M. Militzer, and J.F. Bussière: *Scripta Mater.*, 1998, vol. 39, pp. 735–41.
27. A. Smith, S.E. Kruger, J. Sietsma, and S. van der Zwaag: *ISIJ Int.*, 2006, vol. 46, pp. 1223–32.
28. C. Capdevila, F.G. Caballero, and C. De Andrés Carcia: *ISIJ Int.*, 2002, vol. 42, pp. 894–902.
29. Y.K. Lee: *J. Mater. Lett.*, 2002, vol. 21, pp. 1253–55.
30. B. de Meester: *ISIJ Int.*, 1997, vol. 37, pp. 537–51.
31. C. Miao, C. Shang, K. Wang, L. Zhang, and S. Mani: *Acta Metall. Sinica*, 2010, vol. 46, pp. 541–46.
32. R. Denys: *Rev. Soudure*, 1994, no. 1, pp. 26–39.